Decomposition of Ethanol and Dimethyl Ether During Chemical Vapour deposition Synthesis of Single-Walled Carbon Nanotubes

Bo Hou[1], Rong Xiang[1,2], Taiki Inoue[1], Erik Einarsson[1,3], Shohei Chiashi[1], Junichiro Shiomi[1], Akira Miyoshi[4], and Shigeo Maruyama[1*]

[1] Department of Mechanical Engineering, The University of Tokyo, Bunkyo, Tokyo, 113-8656, Japan

[2] HKUST-SYSU Joint Laboratory of Nano Materials and Technology, State Key Laboratory of Optoelectronic Materials and Technologies, School of Physics and Engineering, Sun Yat-Sen University, Guangzhou 510275, China

[3] Global Center of Excellence for Mechanical Systems Innovation, The University of Tokyo, Bunkyo, Tokyo, 113-8656, Japan

[4]Department of Chemical System Engineering, The University of Tokyo, Bunkyo, Tokyo, 113-8656, Japan

[*]E-mail address: maruyama@photon.t.u-tokyo.ac.jp

Abstract

In this study, we investigated carbon feedstock decomposition conditions on the synthesis of single-walled carbon nanotubes (SWNTs) by chemical vapour deposition. We simulated gas-phase thermal decomposition of ethanol and dimethyl ether (DME) at typical SWNT growth conditions using the chemical kinetic model, and confirmed the reaction trends and primary products using Fourier transform infrared (FT-IR) spectroscopy. Molar fractions were correlated against residence time in the reactor by adjusting the volumetric gas flow rate, and concentration profiles of reaction species were compared to the predicted decomposition mechanism. Signature peak intensities indicated concentrations of both ethanol and DME.

1. Introduction

Due to their nanoscale structure and outstanding mechanical, thermal, and electronic properties, single-walled carbon nanotubes (SWNTs) have long been one of the central topics in nanotechnology research. The preparation of high-quality SWNTs with high yield has been the goal of many research endeavours, and great efforts have been made to optimize the production of SWNTs. Currently, arc discharge, laser ablation, and chemical vapour deposition (CVD) are the three main methods for SWNT production. Among these methods, CVD has proven to be the most effective in terms of productivity and controllability.[1)] We have developed an alcohol catalytic CVD (ACCVD) method in which high-purity SWNTs are synthesized using a novel carbon source, alcohol.[2)] The alcohol's OH group is believed to efficiently remove amorphous carbon during the synthesis process.

During CVD formation of a SWNT, a carbon-containing molecule decomposes on the surface of a catalyst nanoparticle. The carbon precipitates from the surface or bulk of the catalyst particle to form a tubular structure. There have been extensive explorations on the influence of the type of carbon feedstock, catalyst, and operation parameters such as temperature and pressure.[2-5)] In the case of ACCVD, alcohol can undergo significant thermal decomposition before ever reaching the catalyst,[6)] so in addition to the CVD parameters, the extent of thermal decomposition is also important; this can have a strong influence on the real gas composition around the catalyst, which will undoubtedly affect SWNT growth. Until now, however, almost no attention has been paid to the thermal decomposition processes occurring before the carbon precursor arrives at the catalyst.

In this work we systematically studied the thermal decomposition of ethanol under typical CVD conditions using both numerical and experimental approaches. Since

SWNTs can be obtained even when ethanol is thoroughly decomposed, we proposed using dimethyl ether (DME)---an isomer of ethanol---as a potential candidate for SWNT synthesis. This is based on the similar decomposition rates and some common products between DME and ethanol. However, DME offers two potential advantages over ethanol as a carbon precursor. Different to ethanol, DME is in the gas phase at room temperature, which allows it to be more easily used in heterogeneous reactions. This makes it simpler to manage, particularly in large-scale systems. Secondly, since its combustion has been reported to produce very little soot[7] DME may yield even cleaner SWNTs than can be synthesized from alcohol. Here we report the synthesis of SWNTs from DME, as well as the influence of temperature and pressure on the thermal decomposition of DME. These findings will be useful for understanding the complicated reaction pathways leading to the formation of SWNTs.

2 Simulation and Experiments

2.1 Simulation

Simulation of the carbon source decomposition process was performed using SENKIN,[8] a computer program that predicts the time-dependent chemical-kinetic behaviour of a homogeneous gas mixture in a closed system. This has been incorporated into CHEMKIN-II,[9] which is a package of computer codes for the analysis of gas-phase chemical kinetics. Constant-temperature and constant-pressure conditions were chosen for the calculations using temperatures and pressures that had been experimentally found to be optimum for SWNT growth. A DME oxidation kinetic model[10] was used without modification.

2.2 Experimental measurements

Concentrations of gas species were estimated from peak intensities in Fourier

transform infrared (FT-IR) spectra. We note that these measurements were made from gas sampled downstream of the CVD apparatus, rather than *in situ*. DME or ethanol was flowed through the quartz tube chamber, which was maintained at a stable temperature and pressure. The temperature profile in the quartz tube during typical CVD at 800 ^{o}C has been studied previously,[6] and the entrance length into the heated region is known to be very short, even at flow rates exceeding those used in this study. This means the carbon feedstock is heated to 800 °C very soon after entering the CVD chamber. The residence time in the heated region was fixed by adjusting the gas flow rate, and the time-history was measured by identifying the concentrations of carbon feedstock based on FT-IR spectra.

The residence time can be calculated from the ideal gas equation, $PV = nRT$. The volume of reactor V can be calculated from the dimensions of our equipment, where the inner diameter of the quartz tube is 2.54 cm and the length from entering the furnace until reaching the substrate position is 30 cm. The pressure P and temperature T were fixed at 1.3 kPa and 1073 K, respectively, so the remaining parameter to be found is amount of substance n, where

$$n = \frac{V_{gas}}{k}. \tag{1}$$

Here, k is a proportionality constant, V_{gas} is the volume of flow gas, and

$$V_{gas} = Qt, \tag{2}$$

where Q is the volumetric flow rate and t is residence time. For the known flow rate, volume V, pressure P and temperature T, the residence time can be calculated from the following equation:

$$t = \frac{PVk}{QRT}. \tag{3}$$

SWNTs were synthesized on a quartz or silicon substrate by ACCVD using ethanol or

DME as the carbon source. Cobalt and molybdenum catalyst nanoparticles were loaded onto the substrate by a liquid-based dip-coat method. The details and procedures have been described in previous reports.[1,11,12] The as-grown SWNTs were characterized by resonance Raman spectroscopy and SEM observation. *In situ* measurement of the transmitted intensity of a 488 nm laser was used to record the array thickness during growth.[11]

3 Results and Discussion

3.1 Effect of ethanol decomposition on SWNT growth

Fig. 1(a) presents a characteristic Raman spectrum of the SWNTs synthesized at 800 ^{o}C with an ethanol pressure of 1.3 kPa. The strong G peak at 1590 cm^{-1}, weak D peak near 1340 cm^{-1}, and clear peaks in the radial breathing mode (RBM) region confirm the existence of high quality SWNTs. The SWNTs grew perpendicular to the substrate into a forest-like array. The typical flow rate of ethanol was 450 sccm, which corresponds to a residence time of approximately 0.1 s.

Interestingly, when the residence time was increased (achieved by changing the flow rate), SWNT growth curves changed significantly,[13] as shown in Fig. 1(b). Decreasing the flow rate, which increases the residence time of ethanol in the heated region, enhanced both the catalyst lifetime and the final film thickness. Since all other parameters were unchanged, this difference could only be due to the different gas composition. That is, for longer resident times, a larger portion of the ethanol would thermally decompose before reaching the catalyst, affecting SWNT synthesis. The enhanced growth is thus attributed to an increase in the concentration of more active species from the thermal decomposition of ethanol.

3.2 Thermal decomposition of ethanol and DME at constant temperature and pressure

Thermal decomposition of ethanol was calculated using the CHEMKIN-II software package, as described in §2.1. The time-dependent gas composition of ethanol (at 1.3 kPa and 800°C) is shown in Fig. 2(b). Approximately 90% of the ethanol decomposes in 1.5 s, which is consistent with the strong flow rate effect seen in Figure 1b. The major products of ethanol decomposition are C_2H_4, H_2O, C_2H_2, CH_4, CO, and H_2. It is known that C_2H_2 is a highly active precursor for SWNT formation, thus the gas mixture of decomposed ethanol is expected to be an active carbon source.[14)]

From the simulation results for DME decomposition shown in Fig. 2(a), DME was found to be 90% decomposed within 1 second, which is similar to that of ethanol under the same conditions. The major products of DME decomposition are CH_4, CO, and H_2, as well as trace amounts of other species such as CH_3OH and CH_2O. By comparing the breaking positions *a*, *a′*, and *b* of ethanol and DME (Fig. 3), we can determine that ethanol is more likely to form C_2 or CH_3OH, the latter of which can be further decomposed into CH_4, CO, and H_2. For DME, however, there is only one breaking position *b*, thus should produce CH_4, CO, and H_2, as predicted by simulation.

To experimentally verify the simulation results, FT-IR spectra of the decomposed gas (Fig. 4) were obtained. The concentration of the feedstock gas was determined from the relative intensity of a characteristic peak in the spectra. For example, the C-O stretching mode at 1200 cm^{-1} was considered to be the characteristic peak for DME, since this signal is very strong and is not present in any of the decomposition products. The characteristic peak for ethanol was the OH stretching mode found near 3600 cm^{-1} (these data can be found in ref. 6). We compare the species molar-fraction profiles of DME decomposition with those of ethanol in Figure 3. These results are for a furnace

temperature of 800 °C and a feedstock pressure of 1.3 kPa. The relative concentrations of DME measured by FT-IR are in good agreement with the simulation.

At the high temperature condition of our experimental measurement, the decomposition of DME can be approximated as

$$CH_3OCH_3 \rightarrow CH_4 + CO + H_2 \quad (4)$$

This means that for cases in which DME decomposition is ~90% or more (and for no pressure gradent), the outgoing volumetric flow rate becomes three times larger than at the inlet, where only DME existed. The real residence time thus becomes 1/3 of that calculated from the volumetric flow rate at the inlet. This decreasing residence time was considered when calculating the relative concentration of DME based on the FT-IR spectra.

In addition to the decreasing residence time, we also considered potential overlap of FT-IR spectral features of DME with those from decomposition products. This could result in the overestimation of the DME concentration, especially at low DME concentrations and high by-product concentrations. The C-O band, which exists only for DME, avoids this interference. The flow in the reactor, however, is not a fully formed plug flow, especially at low pressures where the diffusion of gas becomes significant, thus some of the DME may escape to the exit faster than the calculated residence time. However, this effect is insignificant due to the small volume of the CVD quartz tube, thus possible diffusion of DME was not considered.

Based on the results of DME decomposition, some of the products are similar to those produced from ethanol decomposition, indicating that DME is a potential carbon source for the growth of SWNTs. More importantly, however, is that although ethanol yields SWNTs with little amorphous carbon, DME is known to produce even less soot

during combustion than ethanol.[7] Therefore, the product grown from DME could be an even cleaner carbon source if the process and synthesis conditions were well optimized.

3.3 Influence of temperature and pressure on thermal decomposition of DME

Some prediction of temperature and pressure influence on the thermal decomposition will be helpful for experimental optimization, so to investigate the temperature dependence we fixed the pressure at 1.3 kPa and performed various time-integrations of DME decomposition. The pressure dependence was similarly investigated by fixing the temperature at 800 °C. Temperature and pressure dependences of DME decomposition are shown in Fig. 5. When the temperature increases to 950 ºC, DME is more than 90% decomposed within 0.1 s, which means CH_4 and CO become the major precursors for SWNT growth. At 800 ºC, the DME concentration decreased very quickly for pressures near 0.5 kPa, whereas less than 15% of DME was decomposed when the pressure was increased from 1 up to 7 kPa. After adjusting both the integration time and experimental conditions (primarily by adjusting the flow rate), results of DME decomposition within 0.1 s at various temperatures and pressures are found to be in good agreement with the simulation results (Fig. 5).

3.4 SWNTs grown using DME as a carbon source

To confirm the potential of DME as a novel carbon source for SWNT synthesis, we replaced ethanol in our conventional ACCVD process with DME. Preliminary results clearly confirm that SWNTs can be synthesized from this new precursor. A resonance Raman spectrum from the DME-synthesized SWNTs is shown in Fig. 6, and no clear difference from ethanol was found. Details regarding SWNT synthesis from DME will be reported elsewhere.

4. Conclusions

Gas-phase thermal decomposition of ethanol and DME was simulated using the chemical kinetic model under typical SWNT growth conditions. Profiles of reaction species concentrations were compared to the predicted thermal decomposition mechanism, which confirmed the simulation reaction trends and products. FT-IR spectroscopy was used to measure the concentrations of species resulting from DME and ethanol decomposition, and the molar fractions were correlated against residence time in the reactor by adjusting the flow rate of the feedstock gas. FT-IR experimental results at various temperatures and pressures were found to be in agreement with corresponding simulations. It was also shown that SWNTs could be synthesized by replacing ethanol with DME.

Acknowledgements

One of the authors (BH) was supported through the Global COE Program "Global Center of Excellence for Mechanical Systems Innovation," by the Ministry of Education, Culture, Sports, Science and Technology, Japan.

References

[1] H. J. Dai, A. G. Rinzler, P. Nikolaev, A. Thess, D. T. Colbert, and R. E. Smalley: Chem. Phys. Lett. **260** (1996) 471.

[2] S. Maruyama, R. Kojima, Y. Miyauchi, S. Chiashi, and M. Kohno: Chem. Phys. Lett. **360** (2002) 229.

[3] Y. Murakami, S. Chiashi, Y. Miyauchi, M. H. Hu, M. Ogura, T. Okubo, and S. Maruyama: Chem. Phys. Lett. **385** (2004) 298.

[4] S. Noda, K. Hasegawa, H. Sugime, K. Kakehi, Z. Zhang, S. Maruyama, and Y. Yamaguchi: Jpn. J. Appl. Phys. **46** (2007) 808.

[5] S. Noda, H. Sugime, K. Hasegawa, K. Kakehi, and Y. Shiratori: Jpn. J. Appl. Phys. **49** (2010) 02BA02.

[6] R. Xiang, E. Einarsson, J. Okawa, T. Thurakitseree, Y. Murakami, J. Shiomi, Y. Ohno, and S. Maruyama: J. Nanosci. Nanotechnol. **10** (2010) 3901.

[7] Z. W. Zhao, M. Chaos, A. Kazakov, and P. L. Dryer: Int. J. Chem. Kinet. **40** (2008) 1.

[8] A. E. Lutz, R. J. Kee, and J. A. Miller: Sandia Report SAND87-8248 (1995).

[9] R. J. Kee, F. M. Rupley, and J. A. Miller: Sandia Report SAND89-8009B (1995).

[10] E. W. Kaiser, T. J. Wallington, M.D. Hurley, J. Platz, H. J. Curran, W. J. Pitz, and C. K. Westbrook: J. Phys. Chem. A **104** (2000) 8194.

[11] S. Maruyama, E. Einarsson, Y. Murakami, and T. Edamura: Chem. Phys. Lett. **403** (2005) 320.

[12] E. Einarsson, M. Kadowaki, K. Ogura, J. Okawa, R. Xiang, Z. Zhang, Y. Yamamoto, Y. Ikuhara, and S. Maruyama: J. Nanosci. Nanotechnol. **8** (2008) 6093.

[13] Figure 1(b) is a modified version of that appearing in ref. 6.

[14] R. Xiang, E. Einarsson, J. Okawa, Y. Miyauchi, and S. Maruyama: J. Phys. Chem.

C **113** (2009) 7511.

Figure captions

Figure 1 (a) Typical Raman spectrum of vertically aligned SWNTs synthesized from ethanol. Insets show an enlarged part of the RBM (upper) and an SEM image (lower) of the SWNT array. (b) Experimentally obtained growth curves obtained at 800 °C for different ethanol decomposition times.

Figure 2 (a) Thermal decomposition of DME at 800 °C and 1.3 kPa calculated using CHEMKIN-II (constant temperature and pressure), show 90% of DME decomposes within approximately 1 s. Values obtained from experimentally measured FT-IR spectra (symbols) are in good agreement with calculations (lines). (b) Profiles for ethanol decomposition under the same conditions are shown by dashed lines.

Figure 3 Chemical band breaking positions of ethanol (left) and DME (right) during decomposition.

Figure 4 FT-IR spectra of DME having undergone different degrees of decomposition; the dashed line indicates heavy decomposition and the solid line light decomposition.

Figure 5 (a) Temperature dependence and (b) pressure dependence of thermal decomposition of DME for various residence times (time-integration) at standard CVD conditions.

Figure 6 Typical Raman spectrum of SWNTs synthesized from DME. Inset shows enlarged RBM region.

Figures

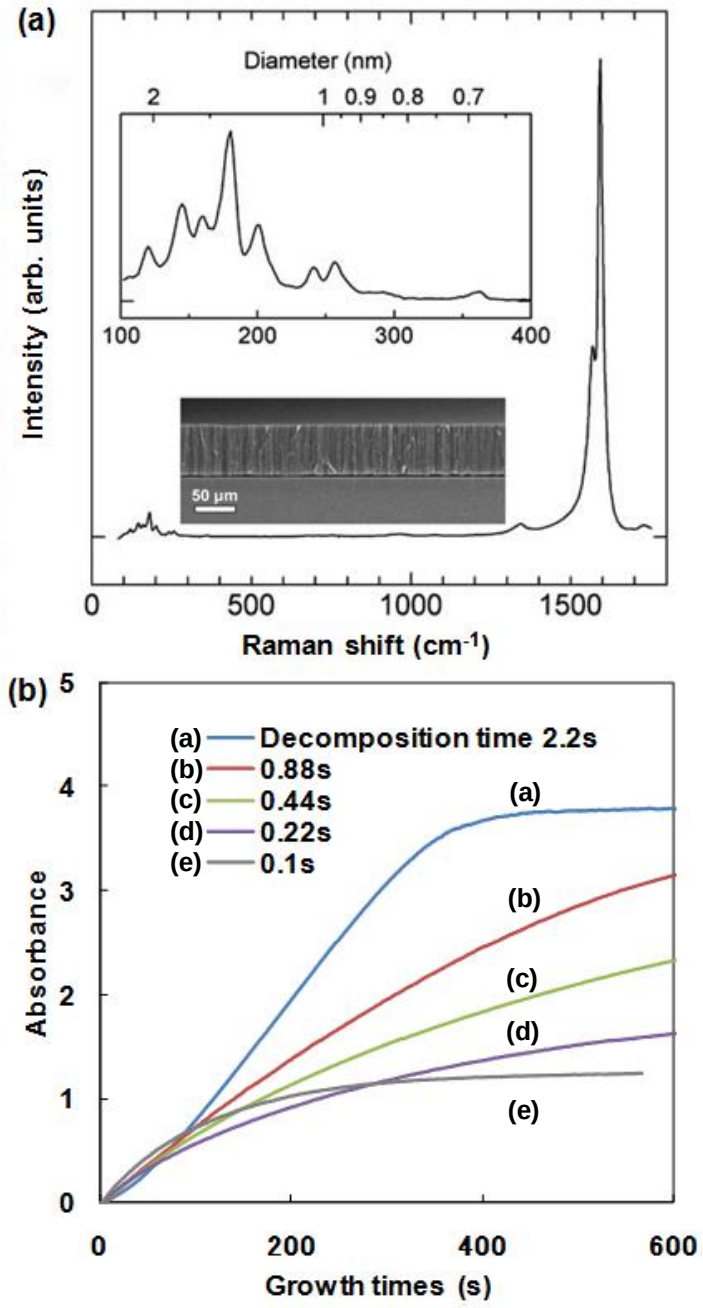

Fig.1

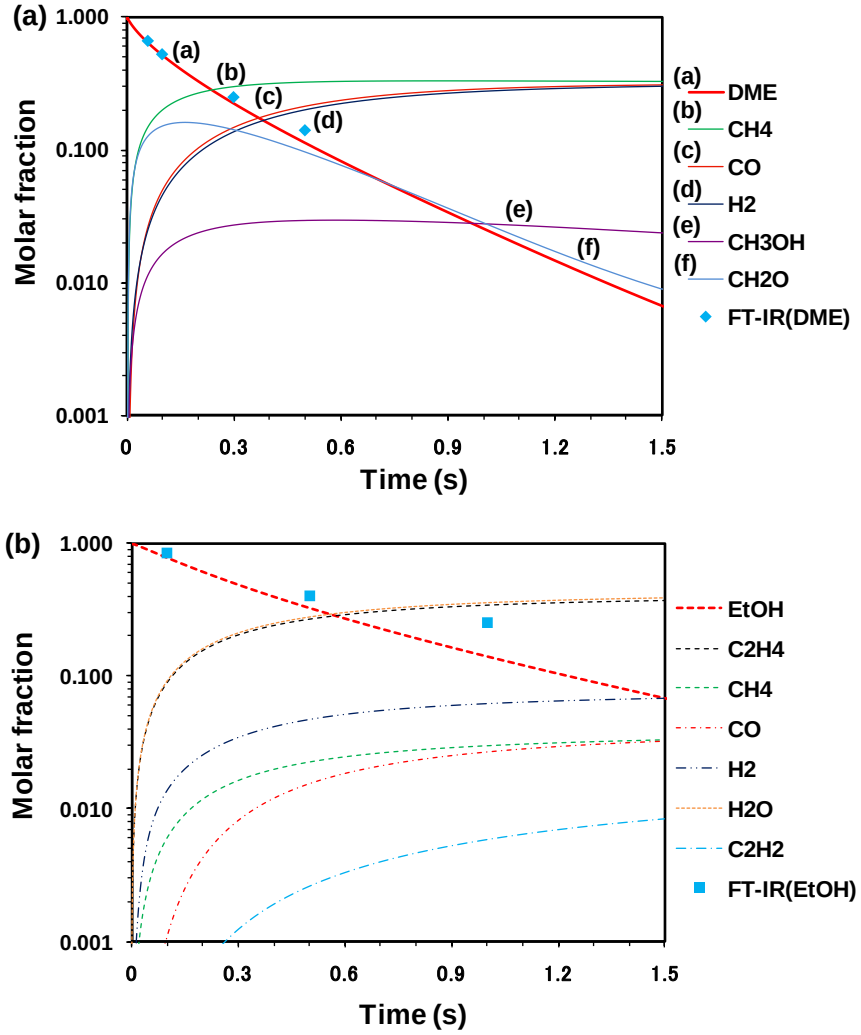
(a)
1.000
0.100
0.010
0.001
Molar fraction
0
0.3
0.6
0.9
1.2
1.5
Time (s)
(a)
(b)
(c)
(d)
(e)
(f)
(a) DME
(b) CH4
(c) CO
(d) H2
(e) CH3OH
(f) CH2O
FT-IR(DME)
(b)
1.000
0.100
0.010
0.001
Molar fraction
0
0.3
0.6
0.9
1.2
1.5
Time (s)
EtOH
C2H4
CH4
CO
H2
H2O
C2H2
FT-IR(EtOH)

Fig. 2

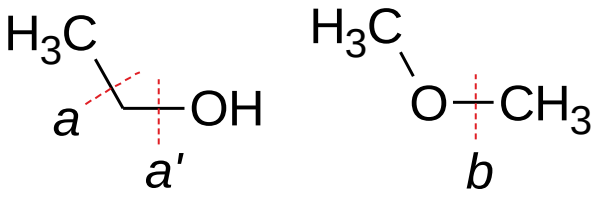

Fig. 3

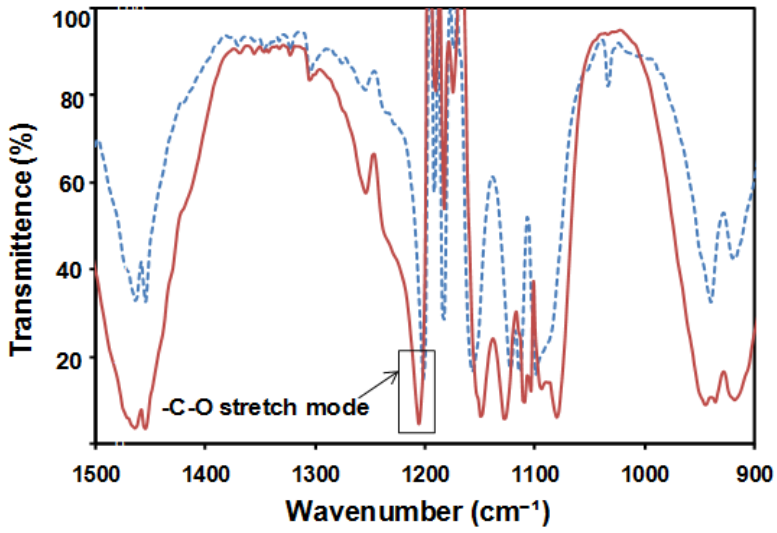
Transmittence (%)
100
80
60
40
20
-C-O stretch mode
1500
1400
1300
1200
1100
1000
900
Wavenumber (cm⁻¹)

Fig. 4

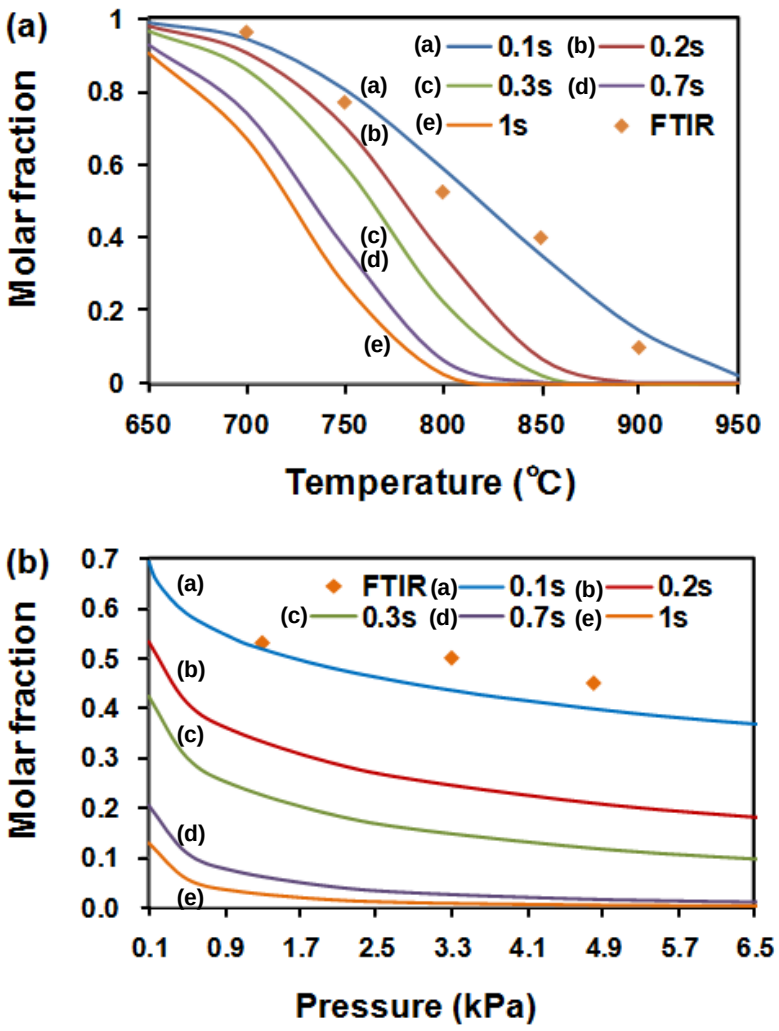
(a)
Molar fraction
1
0.8
0.6
0.4
0.2
0
650
700
750
800
850
900
950
Temperature (℃)
(a) 0.1s (b) 0.2s
(c) 0.3s (d) 0.7s
(e) 1s
FTIR
(a)
(b)
(c)
(d)
(e)
(b)
Molar fraction
0.7
0.6
0.5
0.4
0.3
0.2
0.1
0.0
0.1
0.9
1.7
2.5
3.3
4.1
4.9
5.7
6.5
Pressure (kPa)
FTIR (a) 0.1s (b) 0.2s
(c) 0.3s (d) 0.7s (e) 1s
(a)
(b)
(c)
(d)
(e)

Fig. 5

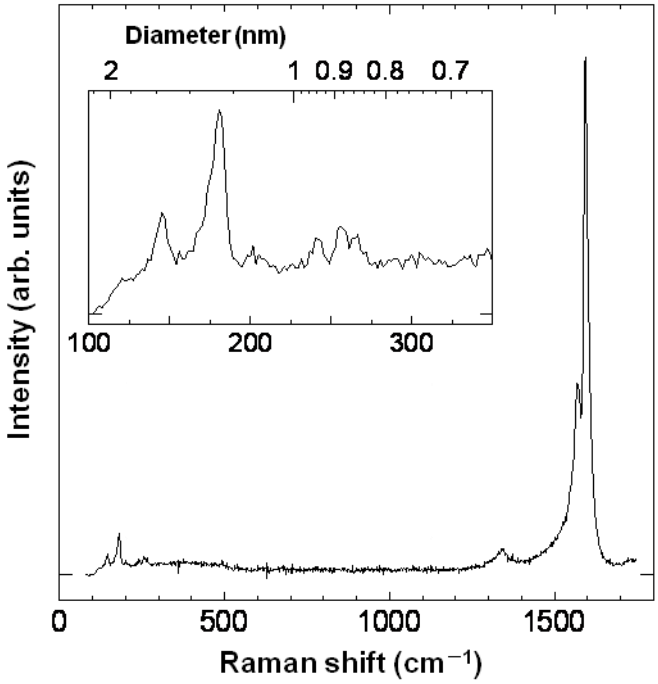
Diameter (nm)
2
1
0.9
0.8
0.7
100
200
300
Intensity (arb. units)
0
500
1000
1500
Raman shift (cm^{-1})

Fig. 6